Journal of Electroceramics, 10, 47–55, 2003

Processing and Electrical Properties of $0.5Pb(Yb_{1/2}Nb_{1/2})O_3$-$0.5PbTiO_3$ Ceramics

CIHANGIR DURAN,* SUSAN TROLIER-McKINSTRY & GARY L. MESSING

Materials Research Institute, Department of Materials Science and Engineering, The Pennsylvania State University, University Park, PA 16802, USA

Submitted March 6, 2002; Revised January 23, 2003; Accepted January 23, 2003

Abstract. $Pb(Yb_{1/2}Nb_{1/2})O_3$-$PbTiO_3$ ceramics at the morphotropic phase boundary (50:50) were sintered by conventional and reactive methods to $\geq$95% theoretical density and grain sizes <10 μm. Excess PbO, added to enhance the densification, resulted in PbO-based non-ferroelectric phases that degraded the electrical properties. Volatilization of excess PbO by annealing the samples after sintering resulted in dense, perovskite samples and excellent electrical properties. The best electrical properties, obtained via reactive sintering, were a remanent polarization, P_r, of 0.36 C/m^2, a maximum dielectric constant of 31,000 (at the $T_c = 371$°C and 1 kHz), a piezoelectric charge coefficient, d_{33}, of 508 pC/N, and an electromechanical coupling coefficient, k_{33}, of 0.61.

Keywords: PYbN-PT ceramics, sintering, ferroelectricity, perovskite, dielectric and elctromechanical properties

Introduction

$Pb(Yb_{1/2}Nb_{1/2})O_3$ was first determined by Smolenskii et al. to be an antiferroelectric material with the perovskite structure [1]. It is a highly ordered complex perovskite and undergoes a sharp antiferroelectric to paraelectric phase transition at the Curie temperature (reported as 280°C in Ref. [1] and 302°C in Refs. [2, 3]). The $(1-x)Pb(Yb_{1/2}Nb_{1/2})O_3$-$xPbTiO_3$ (PYbN-PT) solid solution possesses a morphotropic phase boundary (MPB) region at $x = 0.5$, where it has excellent piezoelectric properties [4]. At room temperature PYbN-PT is an antiferroelectric when $x = 0$, a normal ferroelectric when $x = 0.1$ to 0.15, a relaxor when $x = 0.2$ to 0.49, and a normal ferroelectric when $x > 0.49$. With increasing PT content, ordering of Nb^{5+} and Yb^{3+} on the B site is disturbed and the superlattice structure finally disappears, resulting in normal ferroelectricity [4]. PYbN-PT (50:50) has the highest Curie temperature ($T_c \sim 360$°C) reported among the $Pb(B', B'')O_3$-PT type ceramics, which is due mainly to the high T_c of the PYbN end member [5, 6].

MPB compositions have high dielectric and piezoelectric properties as a result of the large number of polarization directions available. High T_c's at the MPB are desirable because the high piezoelectric coefficients and dielectric constants associated with low T_c's come at the expense of more temperature dependent properties and low depoling temperatures. This, in turn, limits the working range of the devices based on these materials [5]. Therefore, T_c must be considered together with the dielectric and piezoelectric properties of the material in designing more temperature stable ferroelectric devices. Consequently, PYbN-PT ceramics near the MPB are of considerable interest.

PYbN-PT ceramics have been prepared using precalcined, perovskite PYbN-PT powders. In this method, the respective reactants, such as PbO, Yb_2O_3, Nb_2O_5 and TiO_2, were calcined in a single calcination step at 800–900°C [7], or by a two-stage calcination process in which PYbN and PT are separately formed at 800°C prior to a final calcination step at 850°C [4]. In addition, no excess PbO was added to enhance sintering. The best remanent polarization and dielectric constant were 0.33 C/m^2 and $\leq$20,000 (at T_c), respectively [4, 7].

*Present address: Department of Materials Science and Engineering, Gebze Institute of Technology, Gebze, Turkey.

Reactive sintering eliminates the need for calcination step(s) prior to sintering and was shown to enhance densification in $Pb(Mg_{1/3}Nb_{2/3})O_3$-$PbTiO_3$ ceramics [8]. In this method, it is advantageous to use very fine powders to have a high driving force for phase formation and densification at lower firing temperatures. Villegas et al. studied the reactive sintering of $Pb(Zn_{1/3}Nb_{2/3})O_3$-based ceramics and found that higher chemical homogeneity in the reactively sintered ceramics resulted in higher dielectric constants and lower diffusiveness parameters compared to conventionally sintered ceramics [9]. They also mentioned that the pyrochlore grains in the reactively sintered PZN ceramics are isolated and exert less influence on the electrical properties than when interconnected. Duran et al. reported the reactive sintering and enhanced electrical properties in the PYbN-PT ceramics at the MPB. They used two different starting compositions; a mixture of $YbNbO_4$, $PbTiO_3$ and $(PbCO_3)_2{\cdot}Pb(OH)_2$ powders, and a mixture of $YbNbO_4$, TiO_2 and $(PbCO_3)_2{\cdot}Pb(OH)_2$ powders. In both cases, excess $(PbCO_3)_2{\cdot}Pb(OH)_2$ corresponding to 5 wt% PbO was also added as a liquid phase former. The best samples showed a remanent polarization of 0.40 C/m^2, peak dielectric constant of 23,000 (at 1 kHz), and a piezoelectric charge coefficient, d_{33}, of 472 pC/N [10].

The objective of this study was to further explore how various processing factors affect the dielectric, piezoelectric, and electromechanical properties of PYbN-PT ceramics fabricated by reactive and conventional sintering. Densification, phase evolution, and electrical properties were studied as a function of the starting matrix composition, the presence and amount of an initial liquid phase former (0, 3, and 5 wt% excess PbO), sintering temperature (850 to 1050°C for 4 h) and post sintering annealing conditions (800°C for 12 h and 900°C for 4 h).

Experimental Procedure

Ceramic samples of $0.5Pb(Yb_{1/2}Nb_{1/2})O_3$-$0.5PbTiO_3$ (PYbN-PT (50:50)) were prepared by reactive and conventional sintering. In both cases, $YbNbO_4$ was first prepared by ball milling Nb_2O_5 (H.C. Starck) and Yb_2O_3 (Molycorp) powders for 24 h in ethanol. Ethanol was evaporated during fast stirring to eliminate differential settling. The powder mixture was dried at 100°C for 24 h, and then calcined at 1200°C for 4 h. For conventional sintering, a stochiometric mixture of PbO (Alfa), $PbTiO_3$ (Alfa), and $YbNbO_4$ was hand-ground in an alumina mortar and pestle using acetone. This process was repeated two times until the acetone evaporated. The powder mixture was double calcined at 900°C for 3 h to obtain phase-pure PYbN-PT (50:50). Phase formation was checked by X-ray diffraction (XRD) (Rigaku, Japan) using CuKα radiation.

Three reactive compositions were prepared. Two compositions consisted of PYbN and PT and either 3 or 5 wt% excess PbO. PYbN was synthesized by ball milling PbO and $YbNbO_4$ powders for 24 h in ethanol. Ethanol was again evaporated during fast stirring to eliminate differential settling. The powder mixture was dried at 100°C for 24 h, and then calcined at 900°C for 2 h. The third composition was based on $YbNbO_4$, PT, and PbO. Reactive compositions were also prepared by hand-grinding, as described above. Scanning electron microscopy (SEM) showed that the calcined and reground powders were 1–3 μm in diameter. The compositions are summarized in Table 1. Prefixes C and R stand for conventional and reactive sintering, respectively. The final composition for each route was PYbN-PT (50:50).

Pellets were first hand-pressed, with no binder addition, and then cold isostatically pressed at 276 MPa for 15 min. Samples were heated at 5°C/min and sintered in air at 850 to 1150°C for 4 h. During sintering, samples were covered with an Al_2O_3 crucible, a powder mixture of PbO/ZrO_2, and then a second Al_2O_3 crucible in order to minimize lead loss.

The weight change in the samples was determined by measuring the initial and final weights of the samples. Phase formation after sintering was checked by XRD using ground samples. For microstructural analysis, samples were polished to 0.3 μm using fine

Table 1. Sample designation, initial excess PbO content, and the starting matrix compositions.

Designation	Initial excess PbO, wt%	Starting compositions[a]
C0	0	Precalcined $Pb(Yb_{1/2}Nb_{1/2})O_3$-$PbTiO_3$
C3	3	Precalcined $Pb(Yb_{1/2}Nb_{1/2})O_3$-$PbTiO_3$
R3	3	$Pb(Yb_{1/2}Nb_{1/2})O_3 + PbTiO_3$
R5	5	$Pb(Yb_{1/2}Nb_{1/2})O_3 + PbTiO_3$
R5YN	5	$YbNbO_4 + PbO + PbTiO_3$

[a]Final composition for each set is $0.5Pb(Yb_{1/2}Nb_{1/2})O_3$-$0.5PbTiO_3$.

Al_2O_3 powder and then thermally etched for 1 h at 50°C below the sintering temperature. The polished surfaces were cleaned with acetone. The density was measured by the Archimedes technique. Some samples were annealed to remove excess PbO by heating dense samples without any PbO atmosphere control powder. Samples sintered at 850°C for 4 h and 950°C for 4 h were annealed at 800°C for 12 h and 900°C for 4 h, respectively. For the annealing studies, samples were heated quickly (at 10°C/min) so as not to introduce additional sintering.

The surfaces of the samples were polished using 800 grit SiC paper (Leco Corp.) prior to the electrical measurements. For dielectric and piezoelectric measurements, samples were electroded with sputtered platinum. The temperature dependence of the dielectric constant and loss tangent was measured during cooling to room temperature at 2°C/min, using a Hewlett Packard 4284A precision inductance-capacitance-resistance (LCR) meter at frequencies of 1 to 100 kHz. The polarization and coercive field were determined from polarization-electric field (P-E) hysteresis loops recorded at room temperature and 10 Hz, using a modified Sawyer-Tower circuit. Poling was performed at 120°C for 15 min at a field of 4 MV/m. The piezoelectric charge coefficient, d_{33}, of poled samples was measured 24 h after poling, using a Berlincourt d_{33} meter (Model ZJ-2, Institute of Acoustics, China) operating at 100 Hz. The field-induced strain was measured by applying a unipolar electric field to the poled samples at a frequency of 10 Hz.

The longitudinal and transverse electromechanical coupling coefficients (k_{33}, k_{31}) were measured in accordance with the IEEE standards on piezoelectricity [11] using a HP 4194A impedance/gain phase analyzer. From the measured resonance (f_r) and antiresonance (f_a) frequencies, the mechanical compliances (s_{33} and s_{11}) were also calculated. In order to calculate the longitudinal coefficients (k_{33}, s_{33}), the samples were cut to ~6 × 1 × 1 mm and the impedance was measured along the long dimension (poled direction). The transverse coefficients (k_{31}, s_{31}) were obtained from samples with the dimensional ratio of ~5 × 1 × 0.3 mm with the impedance measured on the largest area face (poled direction for a length extensional mode). The f_r and f_a frequencies were determined from the first minimum and maximum impedance peaks in the impedance/frequency scan.

Results and Discussion

Densification, Phase Formation, and Annealing Studies

The relative density and weight change of the samples are tabulated in Table 2 as a function of initial matrix composition, sintering, and annealing conditions. The relative density was calculated on the basis of theoretical density (i.e., 8.43 ± 0.03 g/cm^3) determined from x-ray lattice parameters obtained from powder samples of each composition studied [12]. Note that weight changes in the sintered samples only reflect the changes after those specific sintering conditions. On the other hand, weight changes in the annealed samples show the total weight changes after both sintering and annealing.

Conventionally prepared samples, batched without excess PbO (C0 samples), were only ~80% dense when sintered at 950 or 1050°C for 4 h. When 3 wt% PbO was added (C3 samples), the conventionally sintered samples densified to 96% after 4 h at 850°C but dedensified

Table 2. The % theoretical density and weight change in the samples as a function of initial matrix powder composition, sintering and annealing conditions (− and + signs denote loss and gain after heat treatment, respectively).

	% theoretical density (% loss or gain[a])				
Routes	850°C-4 h	800°C-12 h[b]	950°C-4 h	900°C-4h[b]	1050°C-4 h
C0			80 (−0.1)		79 (−0.6)
C3	96 (−0.1)		96 (+0.7)	95 (−1.7)	91 (−0.9)
R3	97 (−1.3)	96 (−2.3)	96 (−1.5)	95 (−3.1)	92 (+5.4)
R5	96 (−0.3)	95 (−1.4)	94 (−0.3)	92 (−2.7)	93 (−2.5)
R5YN	84 (−0.8)	83 (−1.9)	93 (−0.1)	91 (−3.4)	83 (−3.2)

[a]Weight change after the heat treatment, excluding initial excess values.
[b]Annealing conditions.

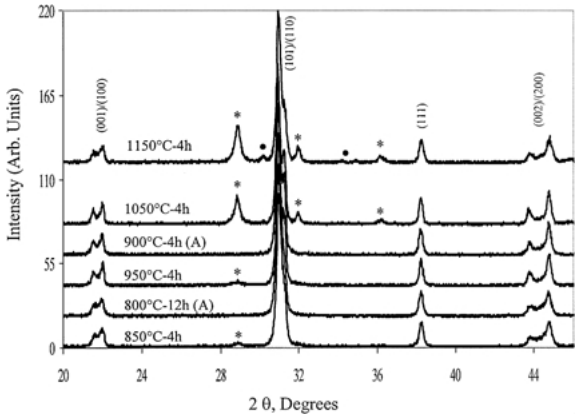

Fig. 1. XRD patterns of the sintered and annealed R3 samples. Samples sintered at 850°C and 950°C were annealed (A) at 800°C and 900°C, respectively. Indexed peaks: perovskite, ∗: PbO, and •: unknown phase.

after sintered at 1050°C for 4 h. Both C0 and C3 samples experienced little weight change below 1050°C, but the C3 samples gained considerable weight at higher sintering temperatures (i.e., +9% after sintering at 1100°C). The relative densification behavior of C0 and C3 samples indicates that excess PbO is necessary to achieve higher densities in conventionally sintered samples. As observed in other excess PbO-containing ceramics, the excess PbO results in liquid phase sintering [13, 14]. Therefore, rearrangement and solution-precipitation mechanisms are activated and thus result in densification at a lower sintering temperature.

Reactively sintered R3 and R5 samples had a similar densification trend but the R5 samples have slightly lower densities, which may be due to the higher liquid phase content. R5YN samples had lower densities and reached a maximum density of 93%, after sintering at 950°C for 4 h (just above the melting temperature of PbO, i.e., 886°C [15]).

Figure 1 shows the XRD patterns of R3 samples as a function of sintering and annealing conditions. The patterns indicate that the compositions are slightly on the tetragonal side of the MPB, based on the splitting in the $\{00l\}$ peaks. Peaks other than perovskite are also marked. Two types of extra peaks are marked. One set of peaks is observed at $2\theta = 28.82$ to 28.94 degrees. These are near the main PbO peaks (JCPDS card #: 35-1482) ($2\theta = 28.74$ degrees) and no other phases in this system occur at that angle. Therefore, these peaks were indexed to the PbO phase. The shift in the peak positions may be due to incorporation of other ions into the PbO lattice [16].

Another set of peaks appears at $2\theta = 30.08$ to 30.20 degrees after sintering at 1150°C. The increased activity of volatile PbO at high temperatures may lead to a decomposition of the perovskite [9], facilitating the conversion to this unknown phase. In fact, pyrochlore formation has not been yet clearly described in PYbN-based ceramics. Yokosuka attributed extra weak peaks in the PYbN-$PbZrO_3$ system to pyrochlore after firing above 1300°C [17]. However, the composition of the phase and the positions of these peaks were not provided. The same extra peaks were also observed in xPYbN-$(1-x)$Pb$(Zr_{0.52}Ti_{0.48})O_3$ compositions when $x \geq 20$ mol% [18]. It was found by x-ray energy dispersive spectroscopy that the second phase was related to the formation of a Yb/Nb mixed compound within the matrix grains, which is possible in our case, too. Table 3 shows the approximate amount of perovskite phase, calculated from the powder XRD patterns using the strongest intensity peaks of perovskite and other phases [19];

$$\%\text{Perovskite} = \frac{I_{\text{Perovskite}}}{I_{\text{Perovskite}} + I_{\text{PbO}} + I_{\text{unknown}}} \times 100 \tag{1}$$

Densification (Table 2) and perovskite phase formation (Table 3) in the reactively sintered R3, R5, and R5YN samples indicate that densification and phase formation take place simultaneously for the R3 and R5

Table 3. Perovskite ratio calculated from XRD patterns as a function of composition, sintering and annealing conditions.

Routes	850°C-4 h	800°C-12 h*	950°C-4 h	900°C-4 h*	1050°C-4 h	1150°C-4 h
C0			100		100	
C3	96		100	100	100	75
R3	97	100	96	100	84	77
R5	94	97	94	100	100	77
R5YN	95	97	94	100	100	77

*Annealing conditions.

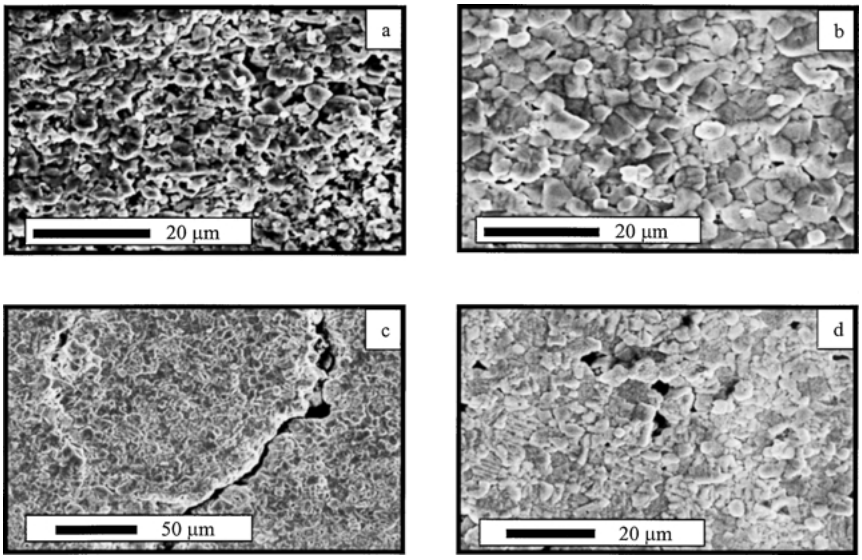

Fig. 2. SEM micrographs of (a) C0, (b) C3, and (c) R3 samples sintered at 1050°C for 4 h, and (d) R5YN sample sintered at 950°C for 4 h.

samples. The R5YN samples, however, are 95% perovskite, but still 84% dense after sintering at 850°C for 4 h. Densification increases sharply to 93% after sintering at 950°C for 4 h, that is, after PbO melts. Because PbO is one of the starting powders in R5YN rather than just a liquid former as in R3 and R5, a possible volume expansion during PYbN formation from PbO and $YbNbO_4$ may retard the densification at lower sintering temperatures. In addition, formation of the final perovskite PYbN-PT solid solution may be easier in R3 and R5 in that both use perovskite PYbN and PT as the starting powders. More study is needed to determine the details of PYbN-PT phase formation in the reactive system.

Annealing studies showed that samples lose different amounts of PbO as a function of their starting compositions, initial amount of excess PbO, and sintering temperature (See Table 2). The perovskite ratio after annealing was always higher than the as-sintered parts (Table 3) because heat treatment without a PbO source can cause excess PbO to volatilize due to the chemical potential difference between the sample and its environment. 5 wt% excess PbO containing samples (R5 and R5YN) showed residual second phases after annealing, but 3 wt% excess PbO samples (R3) were phase-pure perovskite (by XRD) after annealing at 800°C for 12 h. Annealing the samples above the melting point of PbO resulted in more efficient removal of PbO.

Microstructural Analysis

Figure 2 shows a series of SEM micrographs of the C0, C3, and R3 samples sintered at 1050°C for 4 h, and R5YN sample sintered at 950°C for 4 h. The samples had a maximum grain size <10 μm. No exaggerated grain growth was observed, despite varying amounts of initial liquid phase former. The C0 samples sintered at 950 and 1050°C for 4 h were very soft, which is due to the lack of liquid phase sintering. In general, samples annealed at 800°C for 12 h showed an outer shell of light colored material, surrounding a core of darker colored ceramic, presumably because the excess PbO was not removed from the entire sample. Samples annealed at 900°C for 4 h, however, exhibited more uniform coloration. High temperature sintering caused more liquid phase formation. For instance, the R3 samples sintered at 1050°C for 4 h, C3 and R3 samples sintered at 1100 and 1150°C for 4 h had very flat bottom surfaces after sintering. Also, the lower halves were a darker brown color than the upper halves, which indicates the possibility of a compositional inhomogeneity within the samples. In this case, excessive liquid could easily segregate to the bottom. Moreover, this liquid formation caused cracking (e.g., the R3 sample in Fig. 2(c)) and formation of holes (>200 μm) within the samples sintered after 1050°C. Baumler [20] also observed similar shape distortion in the $Pb(Zn_{1/3}Nb_{2/3})O_3$-$PbTiO_3$-$BaTiO_3$ system such

Table 4. Dielectric properties of the samples (at 1 kHz) as a function of composition, sintering and annealing conditions. Measurements are from at least two samples.

	T_c, °C (K at the T_c) $K_{25°C}$ (% $loss_{25°C}$)				
Routes	850°C-4 h	800°C-12 h*	950°C-4 h	900°C-4 h*	1050°C-4 h
C0			386 (8470)		384 (8240)
			940 (2.9)		890 (2.7)
C3	378 (15950)		376 (18610)	371 (24730)	373 (18450)
	1880 (3.0)		1465 (2.9)	1830 (2.9)	1450 (2.7)
R3	375 (23720)	368 (23440)	371 (28000)	371 (31000)	373 (16100)
	1795 (2.8)	1755 (2.8)	1920 (2.4)	1900 (3.0)	1160 (2.0)
R5	379 (16680)	370 (17330)	369 (20180)	375 (19850)	387 (11740)
	1620 (2.8)	1600 (2.9)	1750 (2.8)	1720 (2.9)	1675 (2.3)
R5YN	376 (9650)	368 (11700)	370 (16700)	369 (20210)	369 (11300)
	1260 (3.1)	1250 (3.2)	1510 (2.7)	1515 (3.2)	1245 (2.9)

*Annealing conditions.

that some compositions were either melted or formed a two phase mixture of perovskite and pyrochlore after sintering to 1125°C. In that work, sintering at 1150°C resulted in the formation of 25 to 50% pyrochlore.

Dielectric and Piezoelectric Properties

The dielectric properties (e.g., Curie temperature (T_c), dielectric constant (K) at the T_c and room temperature ($K_{25°C}$)), and dielectric loss at room temperature (%$loss_{25°C}$)) were measured at 1 kHz (Table 4). The C0 samples had the lowest peak dielectric constants (<8,500) among the samples studied. Although these samples were phase-pure perovskite (Table 3), they only reached 80% density. The C3 samples showed the highest dielectric constant ($K_{max} \sim 18{,}500$) when sintered at 950 or 1050°C for 4 h. Annealing at 900°C for 4 h further improved the dielectric constant, K_{max}, to 24,730.

The R3 and R5 samples show a similar trend of dielectric properties and reach their maximum values after sintering at 950°C for 4 h. However, the R5 samples exhibit lower dielectric maxima due to the lower perovskite content and slightly lower densities (see Tables 2 and 3). The R3 sample after annealing at 900°C for 4 h had a K_{max} of 31,000, which was the maximum obtained in this study. In the literature, a $K_{max} \leq 20{,}000$ was reported for conventionally sintered samples [4, 7]. The R5YN samples had a K_{max} after sintering at 950°C for 4 h and then showed a decreasing tendency due to dedensification. Annealing this sample at 900°C for 4 h resulted in improved dielectric constant due to better perovskite purity.

Figure 3 shows the behavior of the dielectric properties as a function of temperature and frequency for the R3 samples. The sample annealed at 900°C for 4 h (denoted as "a") has a sharp transition from ferroelectric to paraelectric at the T_c, while the sample sintered at 1150°C for 4 h (denoted as "b") shows a very broad transition together with a suppressed permittivity. In addition, it shows a very dispersive peak dielectric constant with measuring frequency. The change in the

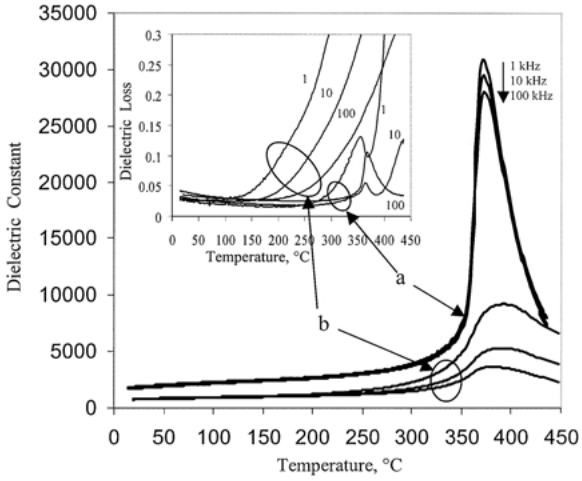

Fig. 3. Effect of the second phases on the dielectric properties of the R3 samples; (a) annealed at 900°C for 4 h after sintering at 950°C for 4 h, (b) sintered at 1150°C for 4 h (the numbers in the inset represent the measuring frequencies in kHz).

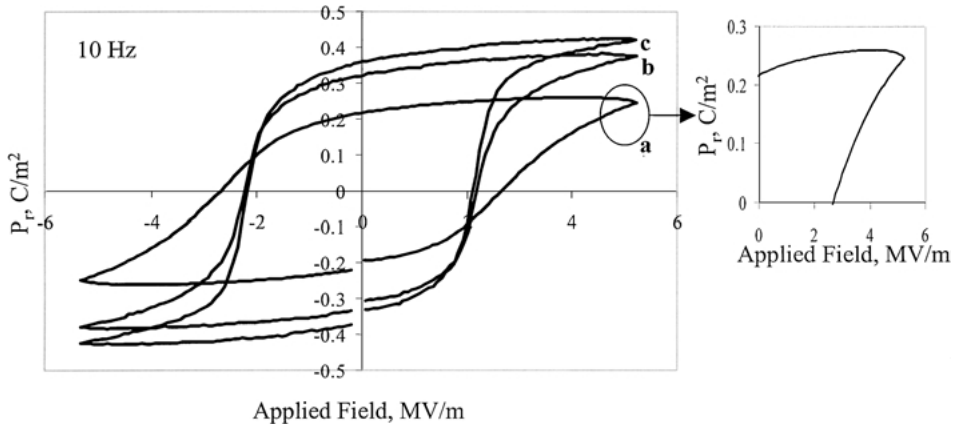

Fig. 4. P-E hysteresis loops of R3 samples; (a) sintered at 1050°C for 4 h, (b) sintered at 950°C for 4 h, and (c) annealed at 900°C for 4 h.

dielectric properties can be attributed to porosity and the presence of nonferroelectric phases. That is, sample "a" has a total (i.e., initial excess PbO content (Table 1) plus weight change (Table 2)) of −0.1 wt% loss compared to a total of +14.5 wt% gain for the sample "b". The inset in Fig. 3 depicts the dielectric loss as a function of temperature and frequency. The dielectric loss increases very sharply well before the T_c for sample "b", which indicates the onset of electrical conduction with temperature due to conductive grain boundary phases. It has been documented in the literature that second phases such as unreacted PbO and PbO-rich phases segregate in the grain boundaries [13, 14, 21]. In general, for all the samples, the dielectric properties were improved after annealing due to elimination of low permittivity, PbO-rich phases from the grain boundaries (e.g., K is ∼26 for PbO [15]).

Figure 4 shows the polarization-field (P-E) hysteresis loops of R3 samples, measured at room temperature and 10 Hz. The loops are well-saturated but become distorted with increasing second phase amount (see inset in Fig. 4 for "a"). The remanent polarization (P_r) and coercive field (E_c) are summarized in Table 5 as a function of composition, sintering and annealing conditions. As expected, the polarization values follow the same tendency as the dielectric properties. The C3 sample annealed at 900°C for 4 h had the highest P_r of 0.34 C/m^2 for conventionally sintered samples. The R3 sample fired at temperatures as low as 850°C had a P_r = 0.35 C/m^2, which is very attractive. Furthermore, it had a slightly higher P_r (0.36 C/m^2) after annealing at 900°C for 4 h. In our previous study [10], a P_r = 0.40 C/m^2 was obtained in samples using $(PbCO_3)_2Pb(OH)_2$ instead of PbO. The reason for the difference may be the initial lead source, because $(PbCO_3)_2Pb(OH)_2$ yields finer PbO particles after decomposition (<550°C), which increases the reaction kinetics and promotes densification at lower temperatures [8]. The best P_r reported in the literature was 0.33 C/m^2 for conventionally sintered samples [4]. In addition, [001] PYbN-0.53PT single crystals have a P_r of ∼0.42 C/m^2 [22].

Table 5. Remanent polarization (P_r) and coercive field (E_c) measured at room temperature, 10 Hz, and 5 MV/m applied field, as a function of composition, sintering and annealing conditions.

	P_r, C/m^2 (E_c, MV/m)				
Routes	850°C-4 h	800°C-12 h*	950°C-4 h	900°C-4 h*	1050°C-4 h
C0			0.24 (2.3)		0.23 (2.4)
C3	0.24 (1.9)		0.27 (2.2)	0.34 (2.2)	0.31 (2.2)
R3	0.35 (2.2)	0.35 (2.2)	0.32 (2.2)	0.36 (2.1)	0.22 (2.7)
R5	0.27 (2.1)	0.30 (2)	0.24 (2.1)	0.23 (2)	0.25 (2)
R5YN	0.17 (1.9)	0.17 (1.8)	0.30 (2.2)	0.31 (2.2)	0.27 (2.2)

*Annealing conditions.

Table 6. Piezoelectric charge coefficient, d_{33} (in pC/N), of the samples measured at 100 Hz and 1 day after poling at 120°C for 15 min and 4 MV/m applied field.

Route	850°C-4 h	800°C-12 h*	950°C-4 h	900°C-4 h*	1050°C-4 h
C0			269		265
C3	175		335	416	397
R3	421	448	477	500	214
R5	309	255	315	372	158
R5YN	174	222	345	385	418

*Annealing conditions.

It has been shown that non-ferroelectric second phases, like PbO, adversely affect the electrical properties. They suppress the dielectric properties, particularly at T_c (Fig. 3), and cause poor polarization and leaky hysteresis loops (Fig. 4) due to conductive grain boundaries, as also observed for other lead-containing ceramics [20, 23, 24].

Poling for all samples was carried out in oil at 120°C. It was found in our earlier study that poling at 2 MV/m resulted in lower d_{33} values because the samples have a coercive field, E_c, around 2.3 MV/m [10]. d_{33} increased with increasing poling field but saturated above 4 MV/m. Therefore, the samples were poled at 120°C for 15 min with an applied field of 4 MV/m. The d_{33} values are summarized in Table 6. The R3 sample, annealed at 900°C for 4 h, has the best d_{33} (500 pC/N) among the samples studied. This sample was further poled for various times at 4 MV/m. d_{33} increased to 506 pC/N after 45 min and to 508 pC/N after 105 min. A d_{33} of 508 pC/N is the highest value reported for $Pb(B'B'')O_3$-PT ceramics with a T_c of 371°C [5]. After poling for 105 min, the same sample was further driven under unipolar condition to observe the strain vs. field behavior (Fig. 5). It shows a hysteretic behavior and the effect of domain reorientation increases with the applied field. A maximum field-induced strain of 0.26% was obtained at 5 MV/m.

In general, the piezoelectric properties of a ferroelectric ceramic can be expressed as,

$$d_{33} \sim 2Q\varepsilon_o\varepsilon P_r \tag{2}$$

where Q is the electrostrictive coefficient, ε_o is the permittivity of free space, ε is the dielectric constant, and P_r is the remanent polarization [5]. The samples with high dielectric constant and remanent polarization had improved d_{33} values, especially after annealing. It was

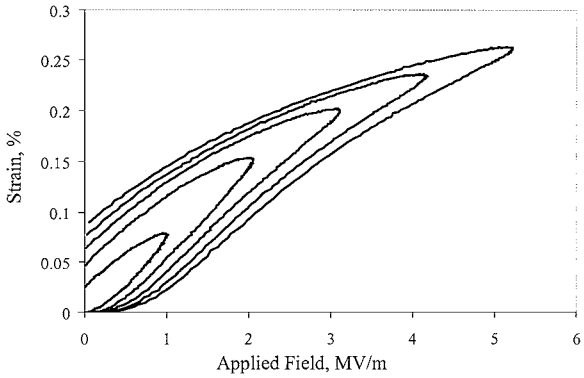

Fig. 5. Graph of strain vs. field for the R3 sample sintered at 950°C for 4 h and annealed at 900°C for 4 h. The sample was poled at 120°C for a total time of 105 min, applying a field of 4 MV/m.

also reported that the dielectric, piezoelectric and electromechanical properties were substantially increased after annealing $Pb(Zn_{1/3}Nb_{2/3})O_3$-$PbTiO_3$-$BaTiO_3$ [20] and $Pb(Zn,Mg)_{1/3}Nb_{2/3}O_3$-$PbTiO_3$ ceramics [21].

IEEE resonance measurements were carried out to investigate the set of low-field properties using the R3 samples annealed 900°C for 4 h. The samples were poled at 120°C for 15 min with an applied field of 4 MV/m. The mechanical compliances (s_{33}^E, s_{33}^D, s_{11}^E, s_{11}^D), the electromechanical coupling coefficients (k_{33}, k_{31}), and d_{31} were calculated from the measured resonant frequency (f_r) and the anti-resonant frequency (f_a) of the sample impedance. Here, the superscripts E and D indicate that the property was measured at constant electrical field and dielectric displacement, respectively. The samples have a $k_{33} = 0.61$, $k_{31} = 0.23$, $d_{31} = -81$ pC/N, $s_{33}^E = 20.57 \times 10^{-12}$ m^2/N, $s_{33}^D = 12.81 \times 10^{-12}$ m^2/N, $s_{11}^E = 15.85 \times 10^{-12}$ m^2/N, and $s_{11}^D = 15.04 \times 10^{-12}$ m^2/N.

It has been shown that electrical properties are very sensitive to the changes in the processing parameters such as density, weight change, and the presence and

amount of a second phase. Therefore, a well-saturated P-E loop, sharp transition from ferroelectric to paraelectric phase at T_c, and lower conduction losses can be obtained from a sample that contains minimal second phases.

Conclusions

PYbN-PT ceramics at the MPB composition (50:50) were conventionally and reactively sintered to $\geq$95% theoretical density, using different starting matrix powder compositions. All samples showed microstructures with grain sizes <10 μm. The presence of a liquid phase increased the densification and subsequent electrical properties for conventionally sintered ceramics. For the reactive routes using the end compounds (PYbN and PT), it was found that a minimum excess PbO ($\sim$3 wt%) is required to achieve higher densities and electrical properties.

The formation of PbO-based non-ferroelectric phases adversely affected the electrical properties. It is believed that excess PbO segregated to the grain boundary, possibly forming continuous layers between the grains, which resulted in increased conductivity and leaky polarization loops. The dielectric properties after sintering, particularly at the T_c, were suppressed considerably due to the low dielectric constants of these phases. Annealing the samples after sintering volatilized the second phases from the grain boundaries, which helped recover some portion of the electrical properties by increasing the perovskite ratio. The improved electrical properties were observed in the dense and perovskite samples with minimal second phase.

The best electrical properties obtained in the reactive sintering routes were a remanent polarization, P_r, of 0.36 C/m^2, a maximum dielectric constant ($K_{\max}$) of 31,000 (at the $T_c = 371^\circ$C and 1 kHz), a piezoelectric charge coefficient, d_{33}, of 508 pC/N, and an electromechanical coupling coefficient, k_{33}, of 0.61. These values are higher than the conventionally sintered samples from our study ($P_r = 0.34$ C/m^2, $K_{\max} = 24{,}730$ at 1 kHz, and $d_{33} = 416$ pC/N), and also those reported in the literature ($P_r = 0.33$ C/m^2, and $K_{\max} \leq 20{,}000$).

Acknowledgment

This work was supported by ONR Grant N00014-98-1-0527. Cihangir Duran gratefully acknowledges the support of the Gebze Institute of Technology (Turkey) for his Ph.D. study in the USA.

References

1. G.A. Smolenskii, A.I. Agranovskaya, S.N. Popov, and V.A. Isupov, *Sov. Phys. Tech. Phys*., **3**, 1981 (1958).
2. Y.M. Poplavko and V.G. Tsykalov, *Sov. Phys. Solid State*, **9**(11), 2600 (1968).
3. J.R. Kwon, C.K.K. Choo, and W.K. Choo, *Japanese Journal of Applied Physics*, **30**(5), 1028 (1991).
4. T. Yamamoto and S. Ohashi, *Japanese Journal of Applied Physics*, **34**(9B), 5349 (1995).
5. S.-E. Park and T.R. Shrout, *IEEE Transactions on Ferroelectrics and Frequency Control*, **44**(5), 1140 (1997).
6. Y. Yamashita, in *The 7th US-Japan Study Seminar on Dielectric and Piezoelectric Ceramics* (Tsukuba, Japan, 181, 1995).
7. H. Lim, H.J. Kim, and W.K. Choo, *Japanese Journal of Applied Physics*, **34**(9B), 5449 (1995).
8. S. Kwon, E.M. Sabolsky, and G.L. Messing, *J. Am. Ceram. Soc*., **84**(3), 648 (2001).
9. M. Villegas, A.C. Caballero, C. Moure, P. Duran, J.F. Fernandez, and R.E. Newnham, *J. Am. Ceram. Soc*., **83**(1), 141 (2000).
10. C. Duran, S. Trolier-McKinstry, and G.L. Messing, *12th IEEE International Symposium on the Applications of Ferroelectrics*, edited by S.K. Streiffer, B.J. Gibbons, and T. Tsunumi (ISAF, 2000), p. 409.
11. "IEEE Standard on Piezoelectricity," IEEE Standard 176-1978. Institute of Electrical and Electronic Engineers, New York (1978).
12. B.D. Cullity, *Elements of X-Ray Diffraction*, 2nd edn. (Addison-Wesley Publishing Company, Inc., 1978).
13. M. Villegas, A.C. Caballero, M. Kosec, C. Moure, P. Durari, and J.F. Fernandez, *J. Mater. Res.*, **14**(3), 891 (1999).
14. S.M. Gupta and A.R. Kulkarni, *J. Mater. Res.*, **10**(4), 953 (1995).
15. *CRC Handbook of Chemistry and Physics*, 66th edn. (CRC Press, Boca Raton, FL, E53, 1985/86).
16. E.M. Sabolsky, Ph.D. Thesis, The Pennsylvania State University (2001).
17. M. Yokosuka, *Jpn. J. Appl. Phys*., **33**(8A), Part 2, L1100 (1994).
18. K.H. Yoon, Y.S. Lee, and H.R. Lee, *J. Appl. Phys.*, **88**(6), 3596 (2000).
19. S.L. Swartz and T.R. Shrout, *Mater. Res. Bull.*, **17**, 1245 (1982).
20. S.L. Baumler, Master Thesis, The Pennsylvania State University (1986).
21. H.M. Jang and K.-M. Lee, *J. Mater. Res.*, **10**(12), 3185 (1995).
22. S. Zhang, S. Rhee, C.A. Randall, and T.R. Shrout, *Jpn. J. Appl. Phys.*, **41**(2A), (2002).
23. H. Fan and H.-E. Kim, *J. Am. Ceram. Soc.*, **84**(3), 636 (2001).
24. M. Antonova, L. Shebanovs, M. Livinsh, J.Y. Yamashita, A. Sternberg, I. Shorubalko, and A. Spule, *J. of Electroceramics*, **4**(1), 179 (2000).